Alternative method to construct equilibrium distribution functions in lattice-Boltzmann method simulation of inviscid compressible flows at high Mach number

K. Qu, C. Shu,* and Y. T. Chew
Department of Mechanical Engineering, National University of Singapore, Singapore 119260
(Received 9 July 2006; published 23 March 2007)

A method is proposed to construct an equilibrium density distribution function in the simulation of compressible flows at high Mach number by the lattice-Boltzmann method. In this method, the conventional Maxwellian distribution function is replaced by a circular function which is very simple and satisfies all needed statistical relations to recover the compressible Navier-Stokes equations. The circular function is then distributed to the lattice velocity directions by Lagrangian interpolation in such a way that all the needed statistical relations are exactly satisfied when the integral in the phase space is replaced by the summation in the context of the lattice-Boltzmann (LB) method. In this framework, the equilibrium distribution functions and the associated lattice velocity model can be derived naturally without assuming specific forms. Two LB models with adjustable specific heat ratio, respectively, for one-dimensional (1D) and two-dimensional (2D) compressible flows are shown in the paper. Some test cases of compressible flows with strong shock waves are simulated to validate the present approach. Excellent results are obtained. Note that in the simulation, the total variation diminishing (TVD) scheme was used to capture the discontinuity with coarse mesh.

DOI: 10.1103/PhysRevE.75.036706 PACS number(s): 47.11.−j, 47.40.−x

I. INTRODUCTION

As an alternative method to simulate incompressible flows, the lattice-Boltzmann method (LBM) [1–11], which is developed from the lattice gas automaton (LGA) approach [12–15], has received more and more attention in recent years. The governing equation of the LBM can be written as

$$f_i(\mathbf{x}+\mathbf{e}_i\Delta t, t+\Delta t) - f_i(\mathbf{x},t) = \Omega, \tag{1}$$

where $f_i(\mathbf{x},t)$ is the density distribution function along the ith lattice velocity direction at the physical position $\mathbf{x}$, $\mathbf{e}_i$ is the lattice velocity in the ith direction, and Ω is the collision operator. In the application of the LBM, the Bhatnagar-Gross-Krook (BGK) collision model [16] is often used. As such, Ω can be written as

$$\Omega = \frac{\Delta t[f_i^{eq}(\mathbf{x},t) - f_i(\mathbf{x},t)]}{\tau}, \tag{2}$$

where $f_i^{eq}(x,t)$ is the equilibrium distribution function, which is a function of local density, velocity, and temperature of the flow, and τ is the relaxation time.

In the LBM application, the key issue is the determination of the relaxation time τ and equilibrium distribution function f_i^{eq}. τ can be linked to the viscosity of the fluid through the Chapman-Enskog expansion in such a way that the macroscopic variables such as density, velocity, and pressure computed from the LBM can satisfy the Navier-Stokes equations with second-order accuracy. f_i^{eq} is usually a polynomial simplified from the exponential form of the Maxwellian distribution function. Usually, the quadratic form (second-degree polynomial in terms of particle speed and flow velocity) is used, which can be directly derived by applying the truncated Taylor series expansion to the exponential form of the Maxwellian function in terms of the Mach number [17–19]. Recently, Shan *et al.* [20] presented a theoretical framework for representing hydrodynamic systems through a systematic discretization of the Boltzmann kinetic equation by means of Hermite tensor expansion of the Maxwellian function. On the other hand, f_i^{eq} can be determined in the following way. At first, a polynomial with unknown coefficients is assumed for the equilibrium function. The unknown coefficients are determined by the physical and mathematical constraints such as satisfying the conservation laws and recovering the Navier-Stokes (NS) equation [21]. Based on this idea, Zheng *et al.* [22] proposed a platform, in which the users can design their own lattice velocity models and associated coefficients in the equilibrium distribution function.

Since the quadratic form of f_i^{eq} is simplified from the Maxwellian distribution function by the Taylor series expansion in terms of the Mach number, the coefficient in the equilibrium distribution function depends on the temperature (T). For incompressible isothermal flow, T can be considered as a constant. Thus, the coefficient will not generate a temperature gradient when the Chapman-Enskog multiscale expansion is applied. As a result, Navier-Stokes equations can be well recovered. The natural convection problem can also be treated the same way as temperature change is only considered in the buoyancy force according to the Boussinesq approximation. However, when compressible flow is considered where the temperature is changed, the coefficient in the equilibrium distribution function will generate additional terms of the temperature gradient in the process of Chapman-Enskog expansion, which do not exist in the macroscopic governing equations. This is one of the reasons why the conventional equilibrium distribution function cannot be applied to compressible flow. Another reason is the limitation of the small Mach number resulting from the Taylor series expansion in terms of the Mach number. To apply the technique of the LBM for simulation of compressible flows, some attempts have been made. Yan *et al.* [23] proposed a two-

*Corresponding author. Electronic address: mpeshuc@nus.edu.sg

dimensional (2D) 9-bit model with two rest energy levels, which can recover the Euler equation with the streaming-collision process. The Sod and Lax shock tube problem was successfully simulated by this model. Its drawback is that there are a number of free parameters in the model to be specified. Shi *et al.* [24] also constructed a 2D 9-bit model which can recover the Euler equation. The form of f_i^{eq} is assumed to be the same as in the incompressible 2-dimensional 9-bit (D2Q9) model, but the coefficients are chosen differently. The rest energy of particles is also introduced in the model to adjust the specific heat ratio γ. Instead of using the streaming-collision process, a TVD finite difference scheme [25] was used to solve the differential form of the lattice-Boltzmann equation. This method also includes many free parameters which should be chosen carefully to make sure of the positivity of f_i^{eq}. Kataoka and Tsutahara [26] proved that, in the limit of small Knudsen number, the differential form of the lattice-Boltzmann equation could approach the Euler equation in the smooth region, and if the stiff region could not be resolved numerically by a mesh size, it could approach the weak solution of the Euler equation as long as a consistent discretization scheme is used. This important finding implies that discontinuity-capturing schemes should be applied to solve the differential form of the lattice-Boltzmann equation in order to capture discontinuities with a finite number of mesh points. Based on this finding, they developed several models for Euler and NS equations [26,27], and the second-order upwind scheme was used to solve the differential form of the lattice-Boltzmann equation. The drawback of their models is a numerical instability when the Mach number is above 1.

All the above work shows that the use of the Maxwellian distribution function or its equivalent may not be necessary in the LBM simulation of compressible flows. The above work also gives some useful hints for the simulation of compressible flows by the LBM. The first is that, in order to make γ adjustable, the rest energy should be introduced. The second is that it might be more feasible to solve the differential form of the lattice-Boltzmann equation by using finite difference method (FDM), finite volume method (FVM), or finite element method (FEM) for compressible flows with discontinuities. On the other hand, it has to be indicated that so far, only the results of subsonic cases with weak shock waves were presented in these models. The simulation of compressible flows with strong shock waves by the LBM is still a challenging issue. Further work is needed on this development.

Also towards the simulation of compressible flows, Sun and Hsu [28–32] developed the adaptive LBM. In this model, the pattern of lattice velocities varies with the mean flow velocity and the internal energy. This adaptive LBM permits the mean flow to have a high Mach number. A number of compressible flow cases with weak or strong shock waves were successfully simulated by the adaptive LBM. On the other hand, we have to indicate that unlike the conventional LBM, in the adaptive LBM, the density, momentum, and energy are all needed to be transported with nonlinear convection (streaming). τ is fixed as 1 in the adaptive LBM, which may cause some inconvenience for its application. Nevertheless, the adaptive LBM is very illuminative. The equilibrium distribution function in the adaptive LBM has nothing to do with the Maxwellian distribution function, but it can be used to successfully simulate compressible flows. Based on the above work, we may be able to develop some simple equilibrium distribution functions which can recover the compressible Euler and NS equations.

In this work, based on the idea of simplified equilibrium distribution functions of the adaptive LBM, we made a further step to construct an equilibrium distribution function for compressible flows. Different from the adaptive LBM, in our method, the lattice velocity pattern is fixed. And from a circular function, f_i^{eq} and the lattice velocity model are derived naturally without assuming specific forms, which makes f_i^{eq} contain no free parameters. Like the earlier work [24,26,27], the differential form of the lattice-Boltzmann equation is solved by the TVD [25] scheme. Some supersonic flows with weak and strong shock waves were simulated successfully by the present model. In particular, the case of double Mach reflection at Mach number 10 was accurately simulated. Sun and Hsu [28–32] simulated this case with the adaptive LBM where the lattice velocity pattern is not fixed.

The rest of the paper is organized as follows. In Sec. II, our method of constructing the equilibrium distribution function will be described in detail. At first, a simplified equilibrium function is proposed to replace the Maxwellian distribution function as the base of the whole deriving process. Then, by applying the Lagrange interpolation method in the phase space, the equilibrium distribution functions and associated lattice velocity models are derived naturally. Section III presents numerical methods to solve the governing equations in the case of discontinuities. Section IV shows the numerical results and discussion. Finally, Sec. V concludes the paper.

II. METHOD OF CONSTRUCTING EQUILIBRIUM DISTRIBUTION FUNCTIONS IN LBM SIMULATION OF INVISCID COMPRESSIBLE FLOWS

A. Continuum Boltzmann equation and Maxwellian distribution function

The lattice-Boltzmann equation can be derived from integration of the discrete Boltzmann equation, and the discrete Boltzmann equation is from the continuum Boltzmann equation. When the BGK collision model is used, the continuum Boltzmann equation can be written as

$$\frac{\partial f}{\partial t} + \xi \cdot \nabla f = (g - f)/\tau, \tag{3}$$

where f is the density distribution function, g is its corresponding function at equilibrium state, ξ is the particle velocity, and τ is the relaxation time. For the 2D continuum Boltzmann equation, the Maxwellian function [33]

$$g = \rho(2\pi RT)^{-(K+2)/2}\exp\left[-\frac{(\xi_x - u)^2 + (\xi_y - v)^2 + \sum_{k=1}^{K}\xi_k^2}{2RT}\right] \tag{4}$$

is taken as the equilibrium distribution function. Here, ξ_x and ξ_y are the x and y components of the particle velocity, u and v are the mean velocity components, and ξ_k, $k=1,\ldots,K$, are velocities standing for the internal degrees of freedom which include z component velocity, rotational movement velocity, and so on. K is related to the specific heat ratio as $K=(5-3\gamma)/(\gamma-1)+1$ which is 3 for a diatomic gas ($\gamma=7/5$). For the standard LBM which can only simulate isothermal incompressible flows, these internal degrees of freedom are neglected and the Maxwellian function is reduced to

$$g=\rho(2\pi RT)^{-1}\exp\left[-\frac{(\xi_x-u)^2+(\xi_y-v)^2}{2RT}\right].$$

In order for Eq. (3) to recover the conventional Navier-Stokes equation, g should satisfy the following constraints [27]:

$$\int g\,d\xi=\rho, \tag{5}$$

$$\int g\xi_\alpha d\xi=\rho u_\alpha, \tag{6}$$

$$\int g(\xi_\alpha^2+2\lambda)d\xi=\rho(u_\alpha^2+bRT), \tag{7}$$

$$\int g\xi_\alpha\xi_\beta d\xi=\rho u_\alpha u_\beta+p\delta_{\alpha\beta}, \tag{8}$$

$$\int g(\xi_\alpha^2+2\lambda)\xi_\beta d\xi=\rho[u_\alpha^2+(b+2)RT]u_\beta, \tag{9}$$

$$\int g\xi_\alpha\xi_\beta\xi_\chi d\xi=p(u_\alpha\delta_{\beta\chi}+u_\beta\delta_{\chi\alpha}+u_\chi\delta_{\alpha\beta})+\rho u_\alpha u_\beta u_\chi, \tag{10}$$

$$\int g(\xi_\chi^2+2\lambda)\xi_\alpha\xi_\beta d\xi=\rho\{(b+2)R^2T^2\delta_{\alpha\beta}+[(b+4)u_\alpha u_\beta+u_\chi^2\delta_{\alpha\beta}]RT+u_\chi^2u_\alpha u_\beta\}. \tag{11}$$

Here, λ is the average specific rest energy which comes from the internal motion of molecules, b is a positive constant related to the specific heat ratio, γ is $\gamma=(b+2)/b$, and ρ, u, T, p, and R are density, mean velocity, temperature, pressure, and gas constant, respectively. Equations (5)–(7) are mass, momentum, and energy conservation relations, respectively, while Eqs. (8) and (9) are flux relations of momentum and energy. Equations (10) and (11) are the diffusion and dissipation relations of momentum and energy. The resultant compressible Navier-Stokes equations can be written as

$$\frac{\partial\rho}{\partial t}+\frac{\partial\rho u_\alpha}{\partial x_\alpha}=0, \tag{12}$$

$$\frac{\partial\rho u_\alpha}{\partial t}+\frac{\partial\rho u_\alpha u_\beta}{\partial x_\beta}+\frac{\partial p}{\partial x_\alpha}=\frac{\partial P'_{\alpha\beta}}{\partial x_\beta}, \tag{13}$$

$$\frac{\partial\rho\left(\frac{1}{2}u_\alpha^2+bRT\right)}{\partial t}+\frac{\partial\rho\left(\frac{1}{2}u_\alpha^2+bRT\right)u_\alpha+pu_\alpha}{\partial x_\alpha}=\frac{\partial}{\partial x_\beta}\left(k\frac{\partial T}{\partial x_\beta}-P'_{\alpha\beta}u_\alpha\right), \tag{14}$$

where

$$p=\rho RT=\frac{1}{D}\int g(\xi_\alpha-u_\alpha)^2d\xi,$$

$$P'_{\alpha\beta}=\mu\left(\frac{\partial u_\alpha}{\partial x_\beta}+\frac{\partial u_\beta}{\partial x_\alpha}-\frac{2}{3}\frac{\partial u_\chi}{\partial x_\chi}\delta_{\alpha\beta}\right)+\mu_B\frac{\partial u_\chi}{\partial x_\chi}\delta_{\alpha\beta}, \tag{15}$$

and μ is the viscosity, μ_B is the bulk viscosity, and k is the thermal conductivity:

$$\mu=\rho RT\tau,$$

$$\mu_B=2(1/3-1/b)RT\tau,$$

$$k=(1+b/2)\rho R^2T\tau. \tag{16}$$

Since $\gamma=(b+2)/b$, we have

$$\gamma-1=2/b. \tag{17}$$

Thus, the heat conductivity k in Eq. (16) can be written as

$$k=\frac{\gamma R\mu}{\gamma-1}=c_p\mu, \tag{18}$$

which shows that for this model, the Prandtl number is 1—that is, $\Pr=\mu c_p/k=1$. Obviously, the fixed Prandtl number is a disadvantage of the BGK collision model.

B. Circular function as a simple equilibrium distribution function

As shown in Eq. (4), the Maxwellian distribution function is in exponential form. It is not easy to manipulate in the LBM. In this section, we will propose a simple circular function to replace the Maxwellian function as the equilibrium distribution function. For the 2D case, the circular function for g can be defined as

$$g = \begin{cases} \dfrac{\rho}{2\pi c} & \text{if } \|\xi - \mathbf{u}\| = c \equiv \sqrt{D(\gamma-1)e} \quad \text{and } \lambda = e_p = \left[1 - \dfrac{D}{2}(\gamma-1)\right]e, \\ 0 & \text{otherwise,} \end{cases} \tag{19}$$

where e_p is the specific rest energy and $D=2$ is the spatial dimension. The physical meaning of Eq. (19) is that all the mass, momentum, and energy concentrate on a circle located in a 3D space of $\xi_x-\xi_y-\lambda$ as shown in Fig. 1. Here, the rest energy λ is added into the phase space as a new coordinate because the rest energy does not come from the particle transversal velocity. The particle velocity on the circle can be written as

$$\xi = \mathbf{u} + \mathbf{c}, \tag{20}$$

and Eq. (19) gives (2D case)

$$e = \frac{c^2}{2(\gamma-1)} = \frac{bc^2}{4}, \tag{21}$$

$$e_p = [1-(\gamma-1)]e = \frac{bc^2}{4} - \frac{c^2}{2}. \tag{22}$$

As shown in Fig. 1, all the particles are concentrated on the circle. Thus, the integral over the velocity space in Eqs. (5)–(11) is reduced to the one along the arclength of the circle. Along the circle, we have

$$d\xi = ds = c\, d\theta,$$

where θ is the angle of the position vector on the circle with the x axis. For a small arclength ds on the circle, the mass, momentum, and energy are

$$d\rho = \frac{\rho}{2\pi c} ds = \frac{\rho}{2\pi} d\theta,$$

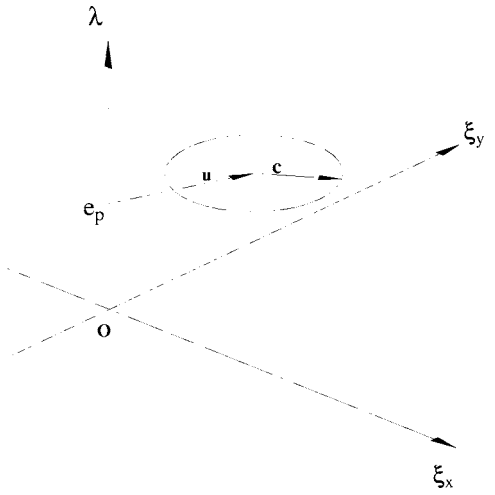

FIG. 1. A circle on the plane of $\lambda=e_p$ in the ξ_x-ξ_y-λ space. $\mathbf{u}$ is the mean velocity, and $\mathbf{c}$ is the effective peculiar velocity.

$$dP_\alpha = \frac{\rho}{2\pi c}(\mathbf{u}+\mathbf{c})_\alpha ds = \frac{\rho}{2\pi}(\mathbf{u}+\mathbf{c})_\alpha d\theta,$$

$$2dE = \frac{\rho}{2\pi c}[(\mathbf{u}+\mathbf{c})_\chi^2 + 2e_p]ds = \frac{\rho}{2\pi}[(\mathbf{u}+\mathbf{c})_\chi^2 + 2e_p]d\theta. \tag{23}$$

Using the formulations

$$\iint d\theta = \int_0^{2\pi} d\theta = 2\pi, \tag{24a}$$

$$\iint \sin\theta d\theta = \int_0^{2\pi} \sin\theta d\theta = 0, \tag{24b}$$

$$\iint \cos\theta d\theta = \int_0^{2\pi} \cos\theta d\theta = 0, \tag{24c}$$

$$\iint \sin^2\theta d\theta = \int_0^{2\pi} \sin^2\theta d\theta = \pi, \tag{24d}$$

$$\iint \cos^2\theta d\theta = \int_0^{2\pi} \cos^2\theta d\theta = \pi, \tag{24e}$$

and Eqs. (17), (21), and (22), we can show that the circular function given by Eq. (19) satisfies the following relations:

$$\int g d\xi = \iint d\rho = \rho, \tag{25}$$

$$\int g\xi_\alpha d\xi = \iint dP_\alpha = \rho u_\alpha, \tag{26}$$

$$\int g(\xi_\alpha^2 + 2\lambda)d\xi = \iint 2dE = \rho(u_\alpha^2 + bRT), \tag{27}$$

$$\int g\xi_\alpha\xi_\beta d\xi = \iint dP_\alpha(\mathbf{u}+\mathbf{c})_\beta = \rho u_\alpha u_\beta + p\delta_{\alpha\beta}, \tag{28}$$

$$\int g(\xi_\alpha^2 + 2\lambda)\xi_\beta d\xi = \iint 2dE(\mathbf{u}+\mathbf{c})_\beta = [\rho u_\alpha^2 + (b+2)RT]u_\beta, \tag{29}$$

$$\int g\xi_\alpha\xi_\beta\xi_\chi d\xi = \iint dP_\alpha(\mathbf{u}+\mathbf{c})_\beta(\mathbf{u}+\mathbf{c}')_\chi = \rho[RT(u_\alpha\delta_{\beta\chi}+u_\beta\delta_{\chi\alpha}+u_\chi\delta_{\alpha\beta}) + u_\alpha u_\beta u_\chi], \tag{30}$$

$$\int g(\xi_\chi^2+2\lambda)\xi_\alpha\xi_\beta d\xi = \iint 2dE(\mathbf{u}+\mathbf{c})_\alpha(\mathbf{u}+\mathbf{c})_\beta = \rho\{bR^2T^2\delta_{\alpha\beta}+[(b+4)u_\alpha u_\beta + u_\chi^2\delta_{\alpha\beta}]RT+u_\chi^2u_\alpha u_\beta\}. \tag{31}$$

In the derivation of Eqs. (25)–(31), we have used the following relations:

$$RT = c^2/2, \tag{32}$$

$$p = \rho c^2/2 = \rho RT. \tag{33}$$

By comparing Eqs. (25)–(31) with Eqs. (5)–(11), it was found that only Eq. (31) has a small difference from Eq. (11) in the coefficient of the first term on the right-hand side. This difference of coefficient only affects the heat conductivity. Similar to Eq. (16), the heat conductivity for the present model is

$$k = b\rho R^2T\tau/2 = R\mu/(\gamma-1) = c_v\mu. \tag{34}$$

Therefore, the Prandtl number in this model is

$$\mathrm{Pr} = \mu c_p/k = c_p/c_v = \gamma. \tag{35}$$

This is the major difference between the use of the circular distribution function and the Maxwellian distribution function. It will not be a problem if we only consider constructing the LB model for inviscid flows.

C. Constraints of discretization from the circular function to a lattice model

It was shown in the above section that the circular function satisfies the constraints (25)–(31) and the compressible Navier-Stokes equation can be recovered with a fixed Prandtl number of γ. However, the circular function cannot be directly applied in the LBM. Although the circular function is greatly simplified as compared to the Maxwellian distribution function, it is still a continuous function and the integral in the phase space is performed along the circle. In the context of the LBM, the discrete lattice velocity is given and fixed in each lattice direction, and the integral in the relevant constraints is replaced by a summation over all lattice velocity directions. It is expected that the equilibrium distribution function in a lattice model can be obtained by discretizing the circular function onto the lattice in such a way that the constraints (25)–(31) can be satisfied in the context of the LBM when the integral is replaced by the summation. In this section, we will study in this process what condition of discretization should be satisfied. It is noted that Eqs. (25)–(29) are needed to recover the Euler equation, while Eq. (301) is required to recover the diffusion term of the momentum (Navier-Stokes) equation and Eq. (31) is needed to recover the diffusion term of the energy equation. Since we only focus on inviscid compressible flow in this study, we will only discuss the constraints (25)–(29).

Suppose that in the $\xi_x-\xi_y-\lambda$ space, there are $1,\ldots,N$ discrete points (lattice velocities in the phase space) $\mathbf{e}_i$. The circular function will be discretized to all $\mathbf{e}_i$ directions. For any $d\rho$ on the circle, it has a contribution $\phi_i(\xi,\lambda)d\rho$ in the lattice direction $\mathbf{e}_i$, where $\phi_i(\xi,\lambda)$ is called the assigning function. The contribution of the whole circle to $\mathbf{e}_i$ direction can be written as

$$\rho_i = \int \phi_i(\xi,\lambda)d\rho = \frac{\rho}{2\pi c}\int \phi_i(\xi,\lambda)ds; \tag{36}$$

ρ_i could be the equilibrium distribution function in the $\mathbf{e}_i$ direction, f_i^{eq}. For convenience, we consider a case in which all $\mathbf{e}_i$ are located on the plane of $\lambda=e_p$. On this plane, $\phi_i(\xi,\lambda)$ can be reduced to $\phi_i(\xi)$. In the context of the LBM, the constraints (25)–(29) can be written as

$$\sum_{i=1}^{N}\rho_i = \iint d\rho, \tag{37}$$

$$\sum_{i=1}^{N}\rho_i e_{i\alpha} = \iint dP_\alpha, \tag{38}$$

$$\sum_{i=1}^{N}\rho_i e_{i\alpha}e_{i\beta} = \iint (dP_\alpha)(\mathbf{u}+\mathbf{c})_\beta, \tag{39}$$

$$\sum_{i=1}^{N}\rho_i(e_{i\chi}^2+2e_p) = \iint 2dE, \tag{40}$$

$$\sum_{i=1}^{N}\rho_i(e_{i\chi}^2+2e_p)e_{i\alpha} = \iint (2dE)(\mathbf{u}+\mathbf{c})_\alpha. \tag{41}$$

$$\sum_{i=1}^{N}\rho_i(e_{i\chi}^2+2e_p)e_{i\alpha} = \int (2dE)(\mathbf{u}+\mathbf{c})_\alpha. \tag{41}$$

Note that the integral in the above equations is along the circle. We can see from Fig. 2 that the discrete velocity $\mathbf{e}_i$ and the original velocity ξ have the following relationship

$$\mathbf{e}_i = \boldsymbol{\xi} + \mathbf{z}_i(\boldsymbol{\xi}). \tag{42}$$

Substituting Eq. (36) into Eq. (37) gives

$$\sum_{i=1}^{N}\rho_i = \iint \frac{\rho}{2\pi c}\sum_{i=1}^{N}\phi_i(\xi)ds \equiv \iint \frac{\rho}{2\pi c}ds. \tag{43}$$

Obviously,

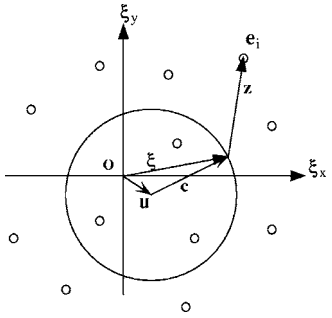

FIG. 2. Configuration of the circle and lattice points in the velocity space. $\mathbf{e}_i$ is one of lattice points, $\mathbf{u}$ is the mean velocity, $\boldsymbol{c}$ is the effective peculiar velocity, and $\mathbf{z}_i$ is the vector from the position on the circle to $\mathbf{e}_i$.

$$\sum_{i=1}^{N} \phi_i(\xi) = 1 \tag{44}$$

is a sufficient condition for Eq. (43). Using Eq. (36), we can also have

$$\sum_{i=1}^{N} \rho_i e_{i\alpha} = \sum_{i=1}^{N} e_{i\alpha} \iint \frac{\rho}{2\pi c} \phi_i(\xi) ds. \tag{45}$$

The above equation can be further written as

$$\begin{aligned}\sum_{i=1}^{N} \rho_i e_{i\alpha} &= \iint \sum_{i=1}^{N} e_{i\alpha} \frac{\rho}{2\pi c} \phi_i(\xi) ds \\ &= \iint \sum_{i=1}^{N} (\xi_\alpha + z_{i\alpha}) \phi_i(\xi) \frac{\rho}{2\pi c} ds \\ &= \iint \frac{\rho}{2\pi c} \xi_\alpha \left[\sum_{i=1}^{N} \phi_i(\xi) \right] ds \\ &\quad + \iint \frac{\rho}{2\pi c} \left[\sum_{i=1}^{N} z_{i\alpha} \phi_i(\xi) \right] ds.\end{aligned} \tag{46}$$

By substituting Eq. (46) into Eq. (38) and using Eq. (44), we obtain

$$\begin{aligned}\sum_{i=1}^{N} \rho_i e_{i\alpha} &= \iint \frac{\rho}{2\pi c} \xi_\alpha ds + \iint \frac{\rho}{2\pi c} \left[\sum_{i=1}^{N} z_{i\alpha} \phi_i(\xi) \right] ds \\ &\equiv \iint \frac{\rho}{2\pi c} \xi_\alpha ds.\end{aligned} \tag{47}$$

A sufficient condition for Eq. (47) is

$$\sum_{i=1}^{N} \phi_i(\xi) z_{i\alpha} = 0. \tag{48}$$

In a similar way, we can get the relationship

$$\begin{aligned}\sum_{i=1}^{N} \rho_i e_{i\alpha} e_{i\beta} &= \iint \frac{\rho}{2\pi c} \xi_\alpha \xi_\beta ds + \iint \frac{\rho}{2\pi c} \left[\sum_{i=1}^{N} z_{i\alpha} z_{i\beta} \phi_i(\xi) \right] ds \\ &\equiv \iint \frac{\rho}{2\pi c} \xi_\alpha \xi_\beta ds,\end{aligned} \tag{49}$$

and its sufficient condition is

$$\sum_{i=1}^{N} \phi_i(\xi) z_{i\alpha} z_{i\beta} = 0. \tag{50}$$

With above formulations (44), (48), and (50), Eq. (40) can be satisfied automatically. Using the same approach, a sufficient condition for Eq. (41) is

$$\sum_{i=1}^{N} \phi_i(\xi) z_{i\alpha} z_{i\beta} z_{i\chi} = 0. \tag{51}$$

Equations (44), (48), (50), and (51) are the constraints for an assigning function $\phi_i(\xi)$. The use of an assigning function to assign a variable from one point to several other points is widely used in particle methods, such as the particle-in-cell method, vortex method, and vortex-in-cell method. It was found [34] that when the third-order Lagrange interpolated polynomial is taken as the assigning function $\phi_i(\xi)$, the constraints (44), (48), (50), and (51) can be satisfied. Thus, in the following, we will discuss the determination of the third-order Lagrange interpolated polynomial on a given stencil which is the lattice in the phase field.

D. Construction of Lagrangian interpolation polynomials

For a two-dimensional case, the complete set of third-order polynomials should have ten terms in the form

$$\begin{aligned}P(x,y) = a_0 + a_1 x + a_2 y + a_3 x^2 + a_4 xy + a_5 y^2 + a_6 x^3 + a_7 x^2 y \\ + a_8 x y^2 + a_9 y^3.\end{aligned} \tag{52}$$

This implies that $\phi_i(x,y)$ should contain at least ten terms. To determine the ten coefficients a_i, $i=0,1,\ldots,9$, Eq. (52) has to be collocated at ten points. For the present problem, these ten points are actually the lattice velocities in the phase field. For all the lattice velocity models in the LBM, there is a static particle with zero lattice velocity and certain moving particles with nonzero lattice velocity. For the ten points in the phase field, one point is for the static particle and the other nine points are for the moving particles. Usually, the nine points would be difficult to form a symmetric lattice when a multispeed lattice velocity model is used. To get a symmetric lattice and, in the meantime, to keep the complete set of third-order polynomials, we may need to use more than ten points in the phase field. Accordingly, we need to add additional higher-order terms to Eq. (52).

The LBM is often applied to the Cartesian mesh, in which the D2Q9 lattice velocity model is well adapted and extensively used. However, this D2Q9 model cannot be applied in this study since it only has nine lattice velocities (nine points in the phase field). We can develop a symmetric lattice based on the D2Q9 model. An example is the D2Q13 lattice model,

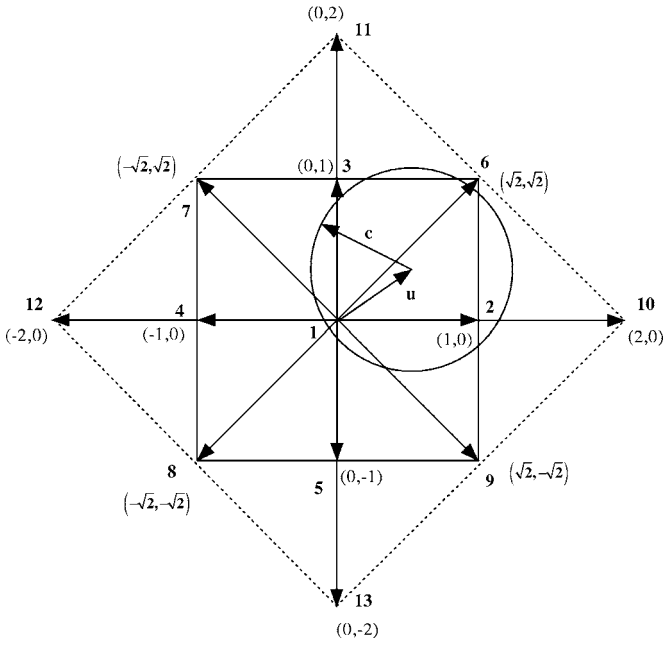

FIG. 3. Configuration of the D2Q13 lattice velocity model.

which is shown in Fig. 3. As compared with the D2Q9 model, the D2Q13 model has four additional velocities (points) $(2,0)$, $(0,2)$, $(-2,0)$, and $(0,-2)$. Consequently, three additional terms $a_{10}x^4+a_{11}x^2y^2+a_{12}y^4$ should be added to Eq. (52) so that when the collocation method is applied, the problem is well posed. The polynomial for the 13 points can be written as

$$P(x,y) = a_0 + a_1x + a_2y + a_3x^2 + a_4xy + a_5y^2 + a_6x^3 + a_7x^2y + a_8xy^2 + a_9y^3 + a_{10}x^4 + a_{11}x^2y^2 + a_{12}y^4. \quad (53)$$

With 13 points, each of the interpolation functions $\phi_i(x,y)$ can be put into the form of Eq. (53). $\phi_i(x,y)$ can be written as

$$\phi_i(x,y) = \mathbf{a}_i\mathbf{t}, \quad (54)$$

where

$$\mathbf{a}_i = [a_{i,1}, a_{i,2}, \ldots, a_{i,13}],$$

$$\mathbf{t} = [1,x,y,x^2,xy,y^2,x^3,x^2y,xy^2,y^3,x^4,x^2y^2,y^4]^T.$$

Once the coefficient vector $\mathbf{a}_i$ is obtained, the interpolation function $\phi_i(x,y)$ is determined. On the other hand, $\phi_i(x,y)$ is a Lagrange-interpolated polynomial, which has the δ property: that is,

$$\phi_i(x_j,y_j) = \delta_{ij}, \quad i,j = 1,2,\ldots,13. \quad (55)$$

The above equation system can be put into the matrix-vector form

$$[A][T] = [I], \quad (56)$$

where

$$[A] = \begin{bmatrix} a_{1,1} & a_{1,2} & \cdots & a_{1,13} \\ a_{2,1} & a_{2,2} & \cdots & a_{2,13} \\ \vdots & \vdots & \ddots & \vdots \\ a_{13,1} & a_{13,2} & \cdots & a_{13,13} \end{bmatrix},$$

$$[T] = [\mathbf{t}(x_1,y_1), \mathbf{t}(x_2,y_2), \ldots, \mathbf{t}(x_{13},y_{13})].$$

$[I]$ is the identity matrix, and (x_j,y_j) are the coordinates of the collocation point. For this study, they are the x and y components of the lattice velocity. It can be seen from Eq. (56) that the coefficient matrix $[A]$ is the inverse of the matrix $[T]$. Once $[A]$ is obtained, the interpolation function $\phi_i(x,y)$ is given by Eq. (55). Using Maple or Mathematica, $\phi_i(x,y)$ can be obtained as follows:

$$\phi_1(x,y) = 1 - 5x^2/4 - 5y^2/4 + x^4/4 + x^2y^2 + y^4/4,$$

$$\phi_2(x,y) = 2x/3 + 2x^2/3 - x^3/6 - xy^2/2 - x^4/6 - x^2y^2/2,$$

$$\phi_3(x,y) = 2y/3 + 2y^2/3 - x^2y/2 - y^3/6 - x^2y^2/2 - y^4/6,$$

$$\phi_4(x,y) = -2x/3 + 2x^2/3 + x^3/6 + xy^2/2 - x^4/6 - x^2y^2/2,$$

$$\phi_5(x,y) = -2y/3 + 2y^2/3 + x^2y/2 + y^3/6 - x^2y^2/2 - y^4/6,$$

$$\phi_6(x,y) = yx/4 + x^2y/4 + xy^2/4 + x^2y^2/4,$$

$$\phi_7(x,y) = -yx/4 + x^2y/4 - xy^2/4 + x^2y^2/4,$$

$$\phi_8(x,y) = yx/4 - x^2y/4 - xy^2/4 + x^2y^2/4,$$

$$\phi_9(x,y) = -yx/4 - x^2y/4 + xy^2/4 + x^2y^2/4,$$

$$\phi_{10}(x,y) = -x/12 - x^2/24 + x^3/12 + x^4/24,$$

$$\phi_{11}(x,y) = -y/12 - y^2/24 + y^3/12 + y^4/24,$$

$$\phi_{12}(x,y) = x/12 - x^2/24 - x^3/12 + x^4/24,$$

$$\phi_{13}(x,y) = y/12 - y^2/24 - y^3/12 + y^4/24. \quad (57)$$

By substituting Eq. (57) into Eq. (36), we can get all ρ_i which satisfy the constraints (37)–(41). However, these statistical relations contain e_p which could be a function of time and physical space. This will bring some inconvenience in applications. Usually, in a lattice model, the lattice properties such as lattice velocity are given and fixed for every physical position and time. As shown in the next section, the drawback of the e_p dependence on time and physical space can be removed by introducing the energy levels in the lattice model.

E. Introduction of energy levels to get fully discrete f_i^{eq}

Since λ is another dimension standing for specific rest energy, with the same idea of assignment, we may introduce several fixed energy levels to assign e_p. As e_p appears lin-

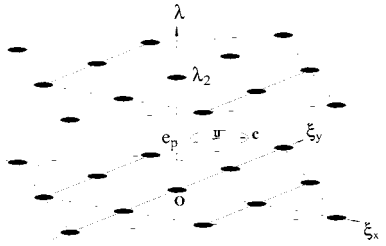

FIG. 4. Configuration of the D2Q13L2 lattice model.

early in Eqs. (40) and (41), conservation of the first-order moment of ρ_i in e_p is enough, which means that only two energy levels are needed, $\lambda_1=0$ and $\lambda_2>e_p$. Linearly assigning every ρ_i onto the two energy levels gives

$$\rho_{i1} = \rho_i(\lambda_2 - e_p)/\lambda_2,$$

$$\rho_{i2} = \rho_i e_p/\lambda_2,$$

which makes $\Sigma_v \rho_{iv}\lambda_v = \rho_i e_p$. Thus ρ_{iv} can satisfy

$$\sum_{i=1}^{N}\sum_{v=1}^{2} \rho_{iv} = \rho,$$

$$\sum_{i=1}^{N}\sum_{v=1}^{2} \rho_{iv} e_{i\alpha} = \rho u_\alpha,$$

$$\sum_{i=1}^{N}\sum_{v=1}^{2} \rho_{iv} e_{i\alpha} e_{i\beta} = \rho u_\alpha u_\beta + \frac{1}{2}\rho c^2 \delta_{\alpha\beta} = \rho u_\alpha u_\beta + p\delta_{\alpha\beta},$$

$$\sum_{i=1}^{N}\sum_{v=1}^{2} \rho_{iv}(e_{i\chi}^2 + 2\lambda_v) = \rho(u_\chi^2 + bRT) = 2\rho E,$$

$$\sum_{i=1}^{N}\sum_{v=1}^{2} \rho_{iv}(e_{i\chi}^2 + 2\lambda_v) e_{i\alpha} = \rho[u_\chi^2 + (b+2)RT]u_\alpha = 2\rho(E+p)u_\alpha, \tag{58}$$

to recover the compressible Euler equations, and we can use ρ_{iv} as f_{iv}^{eq}. By this stage, a 2-dimensional, 13-velocity, 2-energy-level lattice model, named D2Q13L2, is completely derived, and this model is shown in Fig. 4. All the derivations can be implemented with Maple or Mathematica. The Appendix presents detailed formulations of ρ_i and $f_{iv}^{eq}=\rho_{iv}$. Note that λ_2 is not a free parameter. It can be taken as 1 (see the next section) from normalization. This means that there are no free parameters in our lattice model.

F. Chapman-Enskog expansion to recover the Euler equation

It can be easily shown that the present model can make the discrete Boltzmann equation

$$\frac{\partial f_{iv}}{\partial t} + \partial_\alpha(f_{iv}e_{i\alpha}) = -\frac{f_{iv}^{eq} - f_{iv}}{\tau} \tag{59}$$

recover Euler equations with Chapman-Enskog expansion. With Chapman-Enskog expansion, the distribution function is expanded with small disturbance as

$$f_{iv} = g_{iv} + \varepsilon f_{iv}^{(1)} + O(\varepsilon^2) \tag{60}$$

and the following relationship is satisfied:

$$\sum_{i,v}\left[f_{iv}^{(n)}\begin{pmatrix} 1 \\ \mathbf{e}_i \\ \left(\frac{1}{2}\mathbf{e}_i^2 + \lambda_v\right)\end{pmatrix}\right] = 0, \quad n>0. \tag{61}$$

By multiplying Eq. (59) with the collision invariant vector $[1, e_{i\beta}, \frac{1}{2}e_{i\beta}^2+\lambda_v]^T$ and doing summation, we get

$$\sum_{i=1}^{N}\sum_{v=1}^{2}\left\{\left[\frac{\partial f_{iv}}{\partial t} + \partial_\alpha(f_{iv}e_{i\alpha})\right]\begin{bmatrix} 1 \\ e_{i\beta} \\ \frac{1}{2}e_{i\beta}^2 + \lambda_v\end{bmatrix}\right\} = \sum_{i=1}^{N}\sum_{v=1}^{2}\left[\frac{g_{iv}-f_{iv}}{\tau}\right]\begin{bmatrix} 1 \\ e_{i\beta} \\ \frac{1}{2}e_{i\beta}^2 + \lambda_v\end{bmatrix}. \tag{62}$$

By substituting Eqs. (58), (60), and (61) into Eq. (62), we can get macroscopic equations as

$$\frac{\partial}{\partial t}\begin{bmatrix}\rho \\ \rho u_\alpha \\ \rho E\end{bmatrix} + \partial_\alpha\begin{bmatrix}\rho u_\alpha \\ \rho u_\alpha u_\beta + p \\ \rho(E+p)u_\alpha\end{bmatrix} = \partial_\alpha\begin{bmatrix}0 \\ \mathbf{\Pi} \\ \mathbf{q}\end{bmatrix} + O(\varepsilon^2), \tag{63}$$

where

$$\begin{bmatrix}\mathbf{\Pi} \\ \mathbf{q}\end{bmatrix} = -\sum_{i=1}^{N}\sum_{v=1}^{2}\varepsilon f_{iv}^{(1)}\begin{bmatrix} e_{i\alpha}e_{i\beta} \\ e_{i\alpha}\left(\frac{1}{2}e_{i\beta}^2 + \lambda_v\right)\end{bmatrix} \tag{64}$$

are the stress and heat flux resulting from nonequilibrium effects. Since the third-order polynomial is applied, the viscous stress $\mathbf{\Pi}$ can rightly recover $P'_{\alpha\beta}$ in Eq. (15). However, $\mathbf{q}$ cannot recover to the right form. Since we only construct a LB model for inviscid flows for which $f_{iv}=g_{iv}+O(\varepsilon)$, $\mathbf{\Pi}$ and $\mathbf{q}$ can be regarded as artificial dissipation. Thus Eq. (63) can be simplified to

$$\frac{\partial}{\partial t}\begin{bmatrix}\rho \\ \rho u_\alpha \\ \rho E\end{bmatrix} + \partial_\alpha\begin{bmatrix}\rho u_\alpha \\ \rho u_\alpha u_\beta + p \\ \rho(E+p)u_\alpha\end{bmatrix} = \begin{bmatrix}0 \\ O(\varepsilon) \\ O(\varepsilon)\end{bmatrix}. \tag{65}$$

The above derivation process clearly indicates that as long as f_{iv}^{eq} satisfies Eq. (58), the Euler equation can be recovered. Indeed, as shown in the previous section, our proposed equilibrium distribution function satisfies Eq. (58).

III. SOLUTION OF THE DISCRETE BOLTZMANN EQUATION BY THE TVD SCHEME

Since Eq. (3) recovers the Euler equation in the order of $O(\varepsilon)$, the Knudsen number ε should be very small in the numerical simulation. In this case, the dimensionless width of an interface (a shock wave or a contact discontinuity) should be of the order of $O(\varepsilon)$. In order to resolve the interface, the mesh size should be smaller than $O(\varepsilon)$. The use of such a small mesh size is unacceptable. Kataoka and Tsutahara [26] proved that with a finite-difference scheme of pth-order accuracy, Eq. (59) is consistent with the weak form solution of the Euler equation even when the mesh size is much larger than $O(\varepsilon)$ and the error is of the order of $\max(O(\Delta x^p), O(\varepsilon))$. This means that we can solve Eq. (59) on a coarser grid.

To well capture the discontinuity, the numerical computation does need artificial dissipation. The artificial dissipation in the present work comes from two parts. One is the model dissipation which is from the collision term. The other is the numerical dissipation resulting from the TVD discretization. As shown in Eq. (16), the model viscosity μ is related to τ $(=\varepsilon)$. Since τ is taken as very small (10^{-4}) in this work, the model dissipation is also very small and not enough to capture discontinuities without oscillation. So the main dissipation comes from the numerical part—that is, the TVD discretization. In this work, the second-order TVD scheme [35] is used to solve Eq. (59). In the smooth region, the spatial accuracy of the scheme is second order, while near the discontinuity, its accuracy is reduced to first order. For the 2D problem, in the Cartesian coordinate system, the discrete Boltzmann equation can be written as

$$\frac{\partial f_i}{\partial t} + \frac{\partial (f_i e_{ix})}{\partial x} + \frac{\partial (f_i e_{iy})}{\partial y} = -\frac{f_i - f_i^{eq}}{\tau}. \tag{66}$$

Equation (66) is a linear hyperbolic equation system with a source term. It can be solved by the following two steps:

$$\frac{\partial f_i}{\partial t} = -\frac{\partial (f_i e_{ix})}{\partial x} - \frac{\partial (f_i e_{iy})}{\partial y}, \tag{67}$$

$$\frac{\partial f_i}{\partial t} = -\frac{f_i - f_i^{eq}}{\tau}. \tag{68}$$

With the Euler explicit scheme, Eqs. (67) and (68) can be discretized as

$$\frac{f_{i,I,J}^{*} - f_{i,I,J}^{n}}{\Delta t} = -\frac{1}{\Delta x}[F_{i,I+1/2,J}^{n} - F_{i,I-1/2,J}^{n}] - \frac{1}{\Delta y}[G_{i,I,J+1/2}^{n} - G_{i,I,J-1/2}^{n}],$$

$$\frac{f_{i,I,J}^{n+1} - f_{i,I,J}^{*}}{\Delta t} = -\frac{f_{i,I,J}^{*} - f_{i,I,J}^{*eq}}{\tau}, \tag{69}$$

where I and J are indices of mesh points in the x and y directions, respectively, and F and G are numerical fluxes. In this work, a TVD scheme [35] is chosen to evaluate the numerical flux. The scheme can be expressed as

$$\frac{\partial (au)}{\partial x} = \frac{\partial F}{\partial x} = \frac{1}{\Delta x}(h_{I+1/2} - h_{I-1/2}),$$

$$h_{I+1/2} = F_{L,I+1/2} + F_{R,I+1/2},$$

$$F_{L,I+1/2} = F_I^{+} + \frac{1}{2}\min \text{mod}(\Delta F_{I+1/2}^{+}, \Delta F_{I-1/2}^{+}),$$

$$F_{R,I+1/2} = F_{I+1}^{-} - \frac{1}{2}\min \text{mod}(\Delta F_{I+1/2}^{-}, \Delta F_{I+3/2}^{-}),$$

$$F^{+} = 1/2(a + |a|)u,$$

$$F^{-} = \frac{1}{2}(a - |a|)u. \tag{70}$$

In numerical computations, the dimensionless form is preferred. There are three independent reference variables for normalization, which are the reference density ρ_0, reference length L_0, and reference internal energy e_0. With the three reference variables, other reference variables and nondimensional variables can be defined as

$$u_0 = \sqrt{e_0}, \quad t_0 = \frac{L_0}{u_0}, \quad \hat{t} = \frac{t}{t_0},$$

$$\hat{x} = \frac{x}{L_0}, \quad \hat{\rho} = \frac{\rho}{\rho_0}, \quad \hat{u} = \frac{u}{u_0},$$

$$\hat{e} = \frac{e}{e_0}, \quad \hat{f}^{eq} = f^{eq}(\hat{\rho}, \hat{u}, \hat{e}),$$

$$\hat{\tau} = \varepsilon = \frac{\tau}{t_0}, \quad \hat{\lambda}_2 = \frac{\lambda_2}{e_0}. \tag{71}$$

The choice of e_0 is very important. It determines u_0 and normalizes e to $\hat{e}$ from which $\hat{c}$ is computed. As shown in Fig. 3, in order to make sure that the circle is located inside the lattice to avoid extrapolation, we need $|\hat{u}| + |\hat{c}| < \sqrt{2}$ where $\sqrt{2}$ is the shortest distance from the origin to the edges of the D2Q13 lattice. So e_0 should be sufficiently large. For safety, e_0 can be set to a value which is a little bit larger than the maximum stagnation energy in the whole flow field, $e_0 > \max(e^{*})$ where $e^{*} = e(1 + \frac{\gamma - 1}{2}M^2)$. Similarly, λ_2 should also be given a value larger than the maximum e_p in the whole field. In our simulations, we set $\lambda_2 = e_0$ for simplicity, making $\hat{\lambda}_2 = 1$. It makes $\hat{\lambda}_2$ fixed and allows no free parameter in the model. We only need to select e_0 in the computation.

For inviscid flow, the nondimensional relaxation time $\hat{\tau}$ should be very small to recover the Euler equation—for instance, 10^{-3} or 10^{-4} as shown in [26]. For this case, Eq. (66) has a stiff source term. It was found that when the relaxation term is treated explicitly, in order to resolve the relaxation effect, the dimensionless time step $\Delta\hat{t}$ has to be considerably smaller than $\hat{\tau}$, such as $\hat{\tau}/4$ as used in the work of Kataoka and Tsutahara [26]. So the Courant-Friedrichs-Lewy (CFL) number is seriously limited. The implicit integration of the

stiff source term might have a better performance.

The boundary conditions involved in this work are supersonic inflow, supersonic outflow, and reflective wall. For the supersonic inflow, we just need to set $f_i=f_i^{eq}$ computed from the macroscopic variables of ρ, u, v, and e. For the supersonic outflow, the zeroth-order extrapolation is used. On the reflective wall, two levels of ghost cells inside the wall are used and their f_i are determined by

$$f_{i,v,-1} = f_{mirror(i),v,1},$$

$$f_{i,v,-2} = f_{mirror(i),v,2}, \tag{72}$$

where cells -1 and -2 are the ghost cells of cells 1 and 2, respectively, and $mirror(i)$ means the mirror direction of i.

IV. NUMERICAL RESULTS AND DISCUSSION

To validate the proposed model and show its capability for the simulation of compressible flows with shock waves, four standard test cases are considered. These cases either have an exact solution or numerical results given by Euler solvers, which can be used to compare with the present results.

A. Case 1: Sod shock tube

The first test case is the Sod shock tube. This is a one-dimensional problem. All the formulations shown in Sec. II are for the two-dimensional case. Although we can use the 2D model to simulate this 1D case, use of the 1D model can save the computational effort. We can easily follow the same procedure shown in Sec. II to construct a 1D model. For the 1D case, the circular function is reduced to a simpler two-point function—that is,

$$g = \begin{cases} \dfrac{\rho}{2} & \text{if } |\xi - u| = c = \sqrt{D(\gamma-1)e} \quad \text{and } \lambda = e_p = \left[1 - \dfrac{D}{2}(\gamma-1)\right]e, \\ 0 & \text{otherwise}, \end{cases} \tag{73}$$

where $D=1$. Using five-point Lagrange interpolation, we can get a D1Q5L2 model as

$$\rho_1 = \frac{\rho(d_1^2 d_2^2 - d_1^2 u^2 - d_1^2 c^2 - d_2^2 u^2 - d_2^2 c^2 + u^4 + 6u^2 c^2 + c^4)}{d_1^2 d_2^2},$$

$$\rho_2 = \frac{\rho(3d_1 u c^2 - d_1 d_2^2 u - d_2^2 u^2 - d_2^2 c^2 + 6u^2 c^2 + c^4 + u^4 + d_1 u^3)}{2d_1^2(d_1^2 - d_2^2)},$$

$$\rho_3 = \frac{\rho(-3d_1 u c^2 + d_1 d_2^2 u - d_2^2 u^2 - d_2^2 c^2 + 6u^2 c^2 + c^4 + u^4 - d_1 u^3)}{2d_1^2(d_1^2 - d_2^2)},$$

$$\rho_4 = -\frac{\rho(-d_2 d_1^2 u + 3d_2 u c^2 - d_1^2 u^2 - d_1^2 c^2 + 6u^2 c^2 + c^4 + u^4 + d_2 u^3)}{2d_2^2(d_1^2 - d_2^2)},$$

$$\rho_5 = -\frac{\rho(d_2 d_1^2 u - 3d_2 u c^2 - d_1^2 u^2 - d_1^2 c^2 + 6u^2 c^2 + c^4 + u^4 - d_2 u^3)}{2d_2^2(d_1^2 - d_2^2)}, \tag{74}$$

$$f_{i0}^{eq} = \rho_i(\lambda_2 - e_p)/\lambda_2,$$

$$f_{i1}^{eq} = \rho_i e_p/\lambda_2, \tag{75}$$

where $d_1=1$ and $d_2=2$, making the five discrete velocities as $e_i=\{0, d_1, -d_1, d_2, -d_2\}$.

The above equilibrium distribution functions can be used to solve 1D problems. For the problem considered, the initial condition is given as

$$(\rho_L, u_L, e_L) = (1,0,2.5), \quad -0.5 < x < 0,$$

$$(\rho_R, u_R, e_R) = (0.125,0,2), \quad 0 < x < 0.5. \tag{76}$$

In this case, we set $\hat{\tau}=\varepsilon=10^{-4}$, $\rho_0=1$, $L_0=1$, and the reference internal energy $e_0=4>\max(e^*)=2.5$. The mesh size is taken as $\Delta x=1/200$, and the time step size is chosen as $\Delta t=\varepsilon/4$. Before the waves propagate to the two boundary ends, the distribution functions at the boundary can be set as the equilibrium distribution functions computed from the initial value of macroscopic variables. Figure 5 shows the computed density, velocity, pressure, and internal energy profiles (symbols) at $t=0.22$. Also displayed in this figure are the exact solutions (solid lines). Clearly, the present results agree excellently well with the exact solution.

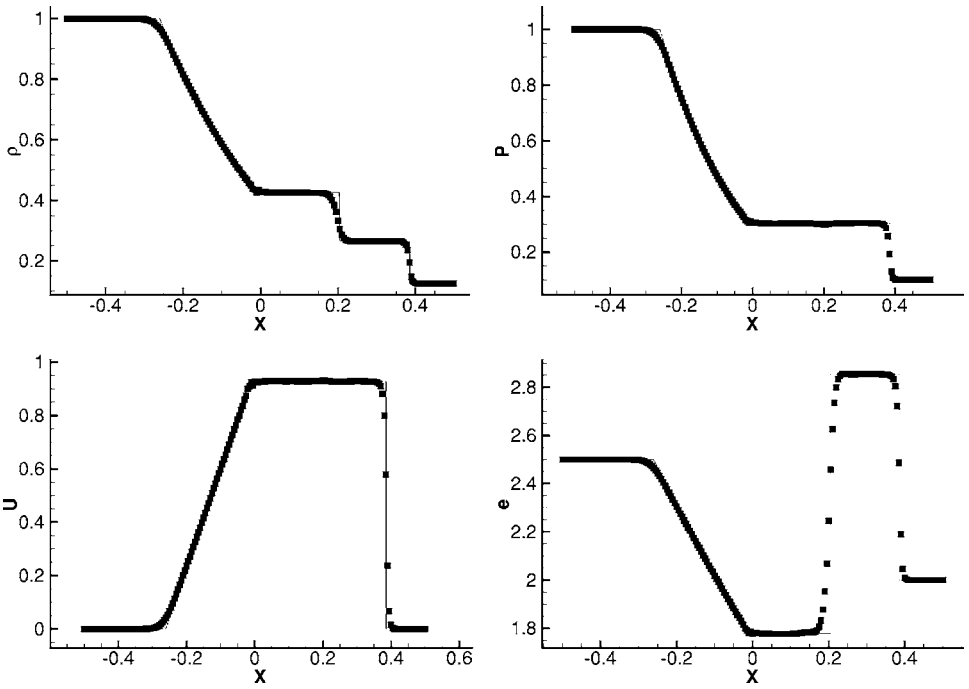

FIG. 5. Density (left up), pressure (right up), velocity (left bottom), and internal energy (right bottom) profiles of a Sod shock tube.

B. Case 2: Lax shock tube

The second test case is the Lax shock tube, which is also a 1D problem and will be solved by the D1Q5L2 model. The initial condition of the problem is given as

$$(\rho_L, u_L, e_L) = (0.445, 0.698, 19.82), \quad -0.5 < x < 0,$$

$$(\rho_R, u_R, e_R) = (0.5, 0, 2.855), \quad 0 < x < 0.5. \tag{77}$$

We set $\varepsilon = 10^{-4}$, $\rho_0 = 1$, $L_0 = 1$, and $e_0 = 30 > \max(e^*) = 19.82$. The mesh size and time step size are taken to be the same as those of the Sod shock tube problem. The computed density, velocity, pressure, and internal energy profiles (symbols) at $t = 0.14$ are shown and compared with the exact solution (solid lines) in Fig. 6. Obviously, the present results are very accurate.

C. Case 3: Shock reflection on a wall

The two shock tube cases presented above are subsonic flow problems. To validate the present model for the simulation of supersonic flows with shock waves, a 2D supersonic flow of shock reflection on the wall is considered. The incoming shock wave with Mach number 2.9 has an incident

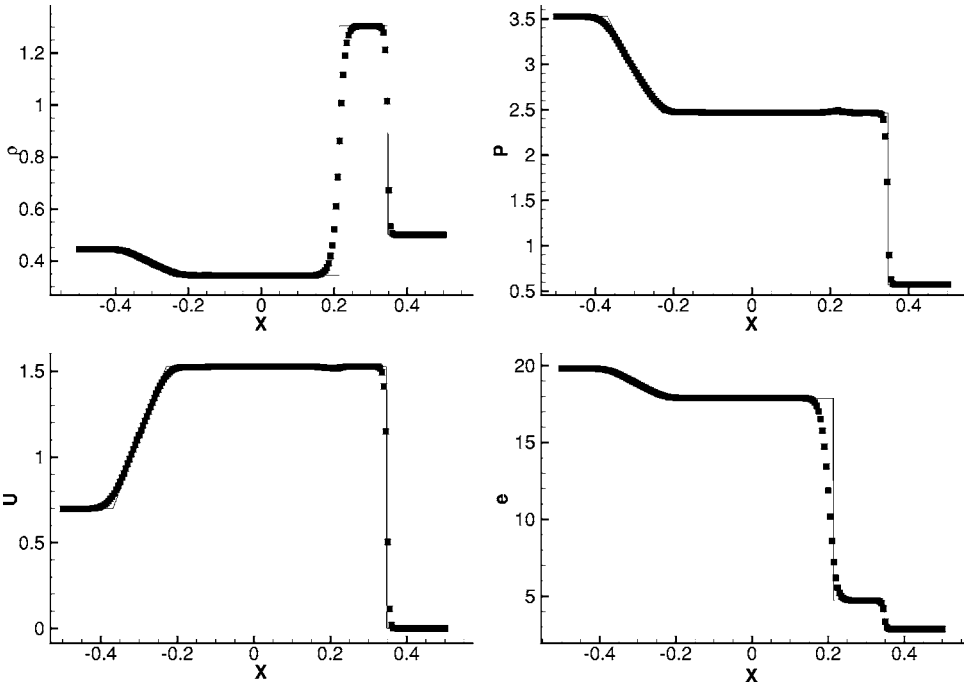

FIG. 6. Density (left up), pressure (right up), velocity (left bottom), and internal energy (right bottom) profiles of a Lax shock tube.

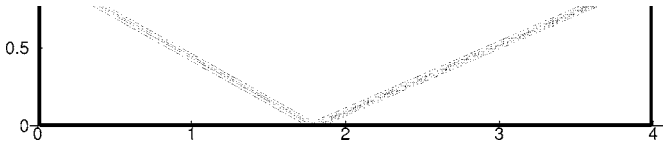

FIG. 7. Density contour of shock reflection on the wall.

angle of 29° to the wall. The computational domain is a rectangle with length of 4 and height of 1. A uniform mesh size of 150×100 is used. The left and top boundary conditions are given by

$$(\rho_L,u_L,v_L,e_L)=(1,2.9,0.0,1.785714),$$

$$(\rho_T,u_T,v_T,e_T)=(1.69997,2.61934,-0.50633,2.247378), \tag{78}$$

and the initial density distribution functions are set as equilibrium values. The right boundary is supersonic outflow where the extrapolation technique is applied. At the wall, the two levels of mirror points are used and the specular boundary condition is applied to consider the velocity slip at the wall. In the computation, we set $\rho_0=1$, $L_0=1$, $e_0=8>\max(e^*)=7.78$, and $\varepsilon=10^{-4}$. Figure 7 presents the computed density contour in which the shock wave is well captured.

D. Case 4: Double Mach reflection

In the above case of shock reflection, the pressure ratio is 2.14, which is not high enough to generate a strong shock wave. In this part, we consider the case of a high-pressure ratio—that is, double Mach reflection (pressure ratio is 116.5)—to show the ability of the present model for simulating a strong shock wave. For this case, a normal shock wave with Mach number 10 passes through a 30° wedge (Fig. 8). A uniform mesh size of 300×100 is used for the numerical simulation. The reference variables are set as $\rho_0=1$, $L_0=1$, $e_0=75>\max(e^*)=72.8$, and $\varepsilon=10^{-4}$. The computed density, pressure, and internal energy contours are shown in Fig. 9. These results are in good agreement with those obtained by using the upwind scheme to directly solve the Euler equation [36]. The complex features such as oblique shocks and triple points are well captured.

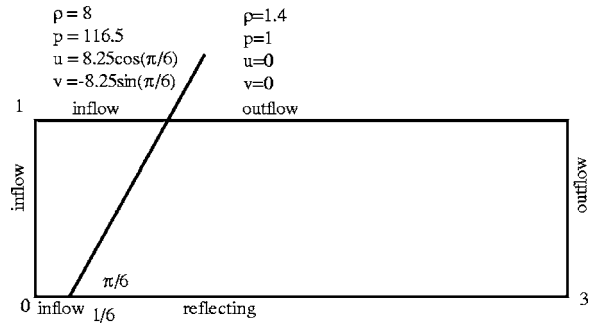

FIG. 8. Configuration of the double-Mach-reflection problem.

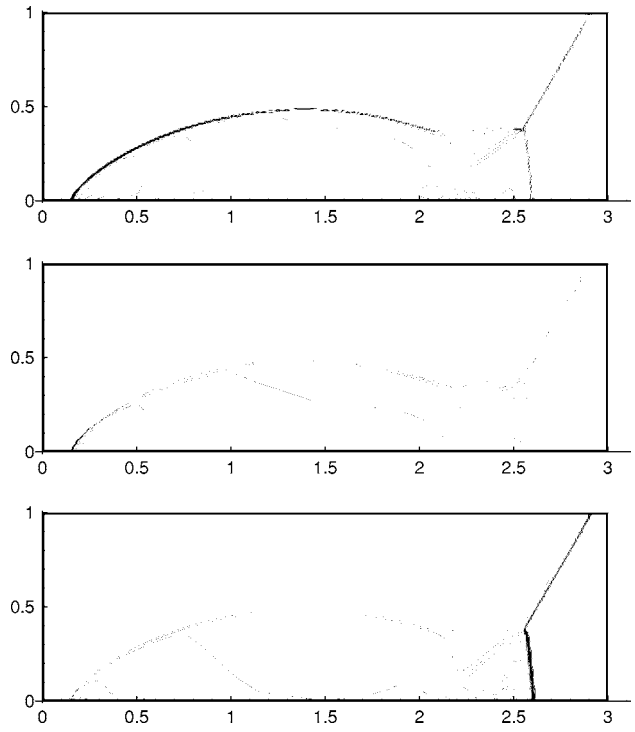

FIG. 9. Density (top), pressure (center), and internal energy (bottom) contours of the double-Mach-reflection problem.

V. CONCLUSIONS

This paper proposes a circular function in the phase field to replace the conventional Maxwellian function as the equilibrium density distribution function. The simple circular function satisfies all statistical relations needed to recover the compressible Navier-Stokes equations. In the context of the lattice-Boltzmann method, the circular function is distributed onto the lattice velocity directions by the Lagrangian interpolation in such a way that all the needed statistical relations are exactly satisfied when the integral in the phase space is replaced by the summation over all lattice velocity directions. In this framework, the equilibrium distribution functions and the associated lattice velocity models are naturally derived. Numerical experiments showed that compressible inviscid flows with strong shock waves can be well simulated by the present model.

APPENDIX: EQUILIBRIUM DENSITY DISTRIBUTION FUNCTIONS OF THE D2Q13 MODEL

Substituting Eq. (57) into Eq. (36) gives

$$\rho_1=1/16\rho(4u^4+5c^4-20c^2+16+16u^2v^2+4v^4-20v^2+20c^2v^2+20c^2u^2-20u^2),$$

$$\rho_2=-1/24\rho(-16u^2+3c^4+4u^4-8c^2+6c^2v^2+12uv^2+18c^2u^2+12c^2u+12u^2v^2-16u+4u^3),$$

$$\rho_3=-1/24\rho(12u^2v^2+6c^2u^2+18c^2v^2+12c^2v+12u^2v+3c^4-8c^2+4v^4-16v^2+4v^3-16v),$$

$$\rho_4 = -1/24\rho(-16u^2 + 3c^4 + 4u^4 - 8c^2 + 6c^2v^2 - 12uv^2 + 18c^2u^2 - 12c^2u + 12u^2v^2 + 16u - 4u^3),$$

$$\rho_5 = -1/24\rho(-4v^3 - 12c^2v - 12u^2v + 3c^4 - 8c^2 + 4v^4 - 16v^2 + 16v + 12u^2v^2 + 18c^2v^2 + 6c^2u^2),$$

$$\rho_6 = 1/32\rho(8uv^2 + 8vu + 4c^2u + 4c^2v + 8u^2v + c^4 + 8u^2v^2 + 4c^2v^2 + 4c^2u^2),$$

$$\rho_7 = 1/32\rho(c^4 + 4c^2v - 8uv^2 - 8vu + 4c^2u^2 - 4c^2u + 4c^2v^2 + 8u^2v^2 + 8u^2v),$$

$$\rho_8 = 1/32\rho(c^4 - 4c^2v - 8uv^2 + 8vu + 4c^2u^2 - 4c^2u + 4c^2v^2 + 8u^2v^2 - 8u^2v),$$

$$\rho_9 = 1/32\rho(c^4 - 4c^2v + 8uv^2 - 8vu + 4c^2u^2 + 4c^2u + 4c^2v^2 + 8u^2v^2 - 8u^2v),$$

$$\rho_{10} = -1/12\rho u + 1/24\rho u^4 - 1/48\rho c^2 - 1/24\rho u^2 + 1/8\rho c^2u^2 + \frac{1}{64}\rho c^4 + 1/12\rho u^3 + 1/8\rho c^2u,$$

$$\rho_{11} = \frac{1}{192}\rho(-16v + 24c^2v - 8v^2 + 8v^4 - 4c^2 + 24c^2v^2 + 16v^3 + 3c^4),$$

$$\rho_{12} = 1/12\rho u + 1/24\rho u^4 - 1/48\rho c^2 - 1/24\rho u^2 + 1/8\rho c^2u^2 + \frac{1}{64}\rho c^4 - 1/12\rho u^3 - 1/8\rho c^2u,$$

$$\rho_{13} = \frac{1}{192}\rho(16v - 24c^2v - 8v^2 + 8v^4 - 4c^2 + 24c^2v^2 - 16v^3 + 3c^4),$$

$$f_{i1}^{eq} = \rho_i(1 - e_p),$$

$$f_{i2}^{eq} = \rho_i e_p,$$

where $e_p = (2-\gamma)e$ and $c = \sqrt{2(\gamma-1)e}$. Note that ρ, u, v, and e are dimensionless variables.

[1] D. A. Wolf-Gladrow, *Lattice-Gas Cellular Automata and Lattice Boltzmann Models* (Springer, Berlin, 2000).
[2] S. Succi, *The Lattice Boltzmann Equation for Fluid Dynamics and Beyond* (Oxford University Press, New York, 2001).
[3] S. Chen and G. D. Doolen, Annu. Rev. Fluid Mech. **30**, 329 (1998).
[4] S. Chen, H. Chen, D. Martinez, and W. H. Mathaeus, Phys. Rev. Lett. **67**, 3776 (1991).
[5] Y. H. Qian, D. d'Humiéres, and P. Lallemand, Europhys. Lett. **17**, 479 (1992).
[6] R. Benzi, S. Succi, and M. Vergassola, Phys. Rep. **222**, 45 (1992).
[7] Y. Chen, Phys. Rev. E **50**, 2776 (1994).
[8] T. Inamuro, M. Yoshino, and F. Ogino, Phys. Fluids **7**, 2928 (1995).
[9] L. S. Luo, Phys. Rev. Lett. **81**, 1618 (1998).
[10] H. Chen, Phys. Rev. E **58**, 3955 (1998).
[11] P. Lallemand and L. S. Luo, Phys. Rev. E **61**, 6546 (2000).
[12] J. Hardy, O. de Pazzis, and Y. Pomeau, Phys. Rev. A **13**, 1949 (1976).
[13] U. Frisch, B. Hasslacher, and Y. Pomeau, Phys. Rev. Lett. **56**, 1505 (1986).
[14] U. Frisch, D. d'Humieres, B. Hasslacher, P. Lallemand, Y. Pomeau, and J.-P. Rivet, Complex Syst. **1**, 649 (1987).
[15] J.-P. Rivet and J. P. Boon, *Lattice Gas Hydrodynamics* (Cambridge University Press, Cambridge, England, 2001).
[16] P. L. Bhatnagar, E. P. Gross, and M. Krook, Phys. Rev. **94**, 511 (1954).
[17] X. He and L.-S. Luo, Phys. Rev. E **56**, 6811 (1997).
[18] X. He and L.-S. Luo, Phys. Rev. E **55**, R6333 (1997).
[19] X. He, S. Chen, and G. Doolen, J. Comput. Phys. **146**, 282 (1998).
[20] X. Shan, X. Yu, and H. Chen, J. Fluid Mech. **550**, 413 (2006).
[21] S. Hou, Q. Zou, S. Chen, G. Doolen, and A. C. Cogley, J. Comput. Phys. **118**, 329 (1995).
[22] H. W. Zheng, C. Shu, Y. T. Chew, and J. Qiu, Int. J. Mod. Phys. C **16**, 61 (2005).
[23] Guangwu Yan, Yaosong Chen, and Shouxin Hu, Phys. Rev. E **59**, 454 (1999).
[24] W. Shi, W. Shyy, and R. Mei, Numer. Heat Transfer, Part B **40**, 1 (2001).
[25] H. C. Yee, J. Comput. Phys. **68**, 151 (1987).
[26] T. Kataoka and M. Tsutahara, Phys. Rev. E **69**, 056702 (2004).
[27] T. Kataoka and M. Tsutahara, Phys. Rev. E **69**, 035701(R) (2004).
[28] C. Sun, Phys. Rev. E **58**, 7283 (1998).
[29] C. Sun, Phys. Rev. E **61**, 2645 (2000).
[30] C. Sun, J. Comput. Phys. **161**, 70 (2000).
[31] C. Sun and A. T. Hsu, Phys. Rev. E **68**, 016303 (2003).
[32] C. Sun and A. T. Hsu, Comput. Fluids **33**, 1363 (2004).
[33] K. Xu, J. Comput. Phys. **171**, 289 (2001).
[34] G.-H. Cottet and P. Koumoutsakos, *Vortex Methods: Theory and Practice* (Cambridge University Press, Cambridge, England, 2000).
[35] H.-X. Zhang, Acta Aerodyna. Sinica **6**, 143 (1988).
[36] P. Colella, J. Comput. Phys. **87**, 171 (1990).